Meccanica (2023) 58:1765–1786
https://doi.org/10.1007/s11012-023-01698-7

Cavitation induced hysteresis of a pitching hydrofoil near free surface

Bing Zhu · Feilin Wang · Luyi Wang

Received: 24 December 2022 / Accepted: 9 August 2023 / Published online: 24 August 2023

Abstract This paper investigates the hysteresis characteristics of force coefficients of an oscillating hydrofoil in a near-free surface cavitation flow field by utilizing unsteady numerical simulation methods. The study primarily focuses on analyzing the effects of dynamic stall conditions, reduced frequency, cavitation number, immersion depth, and Froude number on the hysteresis curve. By comparing the vortex distribution, volume fraction, velocity streamlines, and fluctuating pressure coefficient in the flow field, the authors also examine the reasons for the differences in the hysteresis curve at the same angle of attack under different conditions. The results suggest that cavitation significantly impacts the fluctuation of the hysteresis curve, mainly due to the shedding and collapse of the cavity on the hydrofoil pressure surface, which results in pressure fluctuations at the trailing edge. This issue can be addressed by reducing the stall angle of attack, Froude number, and increasing the reduced frequency, cavitation number, and immersion depth to slow down cavitation in the flow field, thus reducing the fluctuation of the hysteresis loop. Furthermore, the structure of the cavitation flow field under different conditions is clearly distinguished, and the hysteresis loop experiences obvious fluctuations when there is obvious vortex separation in the flow field and many small cavities remaining above the pressure surface. As the immersion depth decreases and the corresponding Froude number increases, the effect of the free surface becomes stronger, leading to an increase in the free surface wave amplitude. This effect causes the hydrofoil pressure surface to gradually evolve into super-cavitation, and the fluctuation of the hysteresis curve tends to be stable.

Keywords Pitching hydrofoil · Cavitation · Dynamic stall · Hysteresis · Free surface

B. Zhu (✉) · F. Wang
University of Shanghai for Science and Technology, Shanghai 200093, China
e-mail: zbing@usst.edu.cn

B. Zhu · F. Wang
Shanghai Key Laboratory of Power Energy in Multiphase Flow and Heat Transfer, Shanghai 200093, China

L. Wang
Science and Technology on Water Jet Propulsion Laboratory, Marine Design and Research Institute of China, Shanghai 200011, China

List of symbols

A	Amplitude of pitch angle
C	Hydrofoil chord length
C_L	Lift coefficient
C_D	Drag coefficient
C_M	Torque coefficient
C_p	Pressure coefficient
d	Free surface distance
ds	Submersion depth
F_D	Drag force
f	Pitch frequency

Fr	Froude number
k	Reduced frequency
F_L	Lift force
M	Torque moment
p_∞	Incoming flow pressure
p_v	Saturated water vapor pressure
Re	Reynolds number
S_t	Strouhal number
SST	Shear stress transfer turbulence model
t	Time
U_∞	Incoming flow speed
VOF	Volume of fluid
V_{vapor}	Volume fraction of vapor
α	Angle of attack
$\overline{\alpha}$	Average angle of attack
ω	Angular velocity
ρ	Density of water
μ	Dynamic viscosity
σ	Cavitation number

1 Introduction

In various applications such as adaptive operating conditions for rotating machinery, flapping hydrofoil propulsion, decreasing drag for high speed sailing, and energy harvesting, the oscillating hydrofoil model is a widely used approximation for describing motion and flow characteristics [1–3]. However, these devices may encounter cavitation when operating near a free surface. Cavitation is a phenomenon that arises due to a phase change when liquid pressure falls to the saturation vapor pressure at a particular temperature. The presence of cavitation can lead to several issues, including reduced device performance [4], structural vibration and noise [5], and erosion damage to the wall surface [6]. Furthermore, cavitation flow itself is an unsteady, multiphase, and complex turbulence [7]. Therefore, investigating cavitation characteristics of oscillating hydrofoils in close to a free surface can provide valuable insights into the interaction between free surfaces and oscillating hydrofoils, help optimize the design and control strategies of underwater propulsion systems, enhance propulsion efficiency and navigation performance, and facilitate the development of novel underwater manipulation systems with higher accuracy and flexibility for use in underwater exploration, operations, and related fields.

Scholars have extensively investigated the phenomenon of static hydrofoil cavitation through numerical and experimental approaches. Sun et al. [8] conducted numerical simulations on the unsteady cavitation shedding dynamics of a hydrofoil in a thermal fluid and observed that the thermal effects can mitigate the intensity of cavitation on the hydrofoil surface and reduce the peak value of pressure fluctuation. The evolution characteristics of the thermal cavitation flow are intricately related to the complex multi-scale vortex structures surrounding the hydrofoil. Ji et al. [9] utilized large-eddy simulation (LES) combined with a uniform cavitation model to simulate the unsteady cavitation turbulent flow around a hydrofoil. Their findings confirmed the relationship between pressure reflection and bubble shedding process and highlighted the volume change rate of the bubble as the primary source inducing pressure fluctuations around the cavitation hydrofoil. Zhao et al. [10] employed LES to investigate the effect of different wavefronts on the cavitation control of a hydrofoil under equal lift conditions. Their results demonstrated that pressure fluctuations could be effectively suppressed, and cavitation was the primary factor affecting the development of flow-induced vortex. Timoshevski et al. [11] utilized high-speed imaging technology, time-resolved laser-induced fluorescence (LIF) visualization technology, 2D particle image velocimetry (PIV) technology, and underwater pressure measurement technology to investigate the efficacy of continuous wall tangential jet injection through the spanwise gap in suppressing hydrofoil surface cavitation. Wang et al. [12] experimentally studied the effect of water injection into the suction surface of a static hydrofoil on cavitation flow. Their findings revealed that water injection can effectively suppress the development of sheet cavitation and cloud cavitation, and injection speed and position have a significant impact on cavitation suppression.

In the field of oscillating hydrofoil cavitation, researchers have conducted various studies. Hart et al. [13]

conducted experimental investigations on the cavitation phenomenon of sinusoidal oscillating hydrofoils and revealed a strong interaction between the natural shedding frequency of the leading-edge cavity and the oscillation frequency of the hydrofoil, resulting in the irregular development of cavitation and violent cavity collapse. Ducoin et al. [14] employed

numerical and experimental approaches to investigate the cavitation of oscillating hydrofoils and reported that the development of hydrofoil surface cavitation is closely associated with the hydrofoil oscillation speed. In addition, increasing the oscillation rate alters the hydrodynamic load and the frequency of bubble generation. Amromin et al. [15] examined the structural vibration features of oscillating hydrofoils under the periodic shedding conditions of cavitation vortices. The findings revealed that the low-frequency and high-frequency components of the hydrofoil vibration are linked to the unsteady cavity evolution process and hydrofoil resonance, respectively. Furthermore, the development and collapse of hydrofoil surface cavitation greatly enhance the structural vibration effect of the hydrofoil. Huang et al. [16] conducted numerical and experimental studies on the influence of hydrofoil oscillation frequency on cavitation flow. The results demonstrated that increasing the oscillation frequency delays the hydrofoil stall and significantly enhances the hydrofoil's behavior after the stall. Kashyap et al. [17] investigated the flow-induced vibration of a free-vibrating hydrofoil under unsteady cavitation conditions through numerical studies. The results indicated the presence of a mechanism that locks the structural frequency to an unsteady lift, thereby maintaining the hydrofoil's high-amplitude vibration. During the frequency locking process, larger coherent cavitation structures were observed on the suction surface of the hydrofoil. Wu et al. [18] developed a fully-cavitating model combined with the VOF method for near-free-surface cavitation hydrofoils. The results demonstrated that although the method has good convergence and can capture the cavitation flow near the free surface, the convergence speed is slow when calculating the cavity shape, particularly in the cavity closure area.

The previous scholars have conducted extensive researches on the dynamic stall and hysteresis effect of oscillating hydrofoils, as well as their hydrodynamic performance. For instance, Zhang et al. [19] and Wu et al. [20, 21] employed Lagrangian coherent structures to investigate the transient flow structure of pitching hydrofoils and effectively predicted and analyzed the dynamic behavior of the flow structure. The results showed that the oscillation frequency of the hydrofoil affects the flow structure and energy extraction efficiency during dynamic stall, and when the oscillation frequency increases, the dynamic stall is delayed, and the total energy extraction efficiency increases. Some scholars have conducted specialized research on the interaction between hydrofoils and free surfaces. Zhang et al. [22] ever used numerical and experimental methods to study the cavitation of oscillating Clark-Y hydrofoils and analyzed its hysteresis curve in three regions. The results showed that the hysteresis curve and cavity shape of the hydrofoil differed in different attack angle regions. Zhu et al. [23] studied the energy extraction performance of a two-dimensional hydrofoil system under a free surface and demonstrated the correlation between the immersion depth and the energy extraction efficiency of the hydrofoil. However, the current research on the cavitation characteristics of oscillating hydrofoils is not sufficiently comprehensive, and there is still a lack of research on the effect of the free surface on the cavitation characteristics of oscillating hydrofoils. This paper employs numerical simulation methods to investigate the dynamic stall characteristics of oscillating hydrofoils under different reduced frequencies, cavitation numbers and free surface distances, by utilizing the NACA 0012 hydrofoil as the research subject. Additionally, the evolution process of the cavitation of the oscillating hydrofoil flow field near the free surface will be analyzed in conjunction with flow field analysis.

2 Physical model and numerical methodology

2.1 Hydrofoil pitching principle

An oscillating hydrofoil was selected as the research object. The pitching center is at a one-quarter chord length from the leading edge of the hydrofoil. The pitching angle, Reynolds number, Froude number and reduced frequency are separately defined as:

$$\alpha = \overline{\alpha} - A\sin(\omega t) \tag{1}$$

$$Re = \frac{\rho U_\infty C}{\mu} \tag{2}$$

$$F_r = \frac{U_\infty}{\sqrt{\mathrm{gC}}} \tag{3}$$

$$k = \frac{\pi f C}{U_\infty} \tag{4}$$

where $\overline{\alpha}$ is the mean angle of attack, A is the amplitude of the pitch angle, the angular velocity is $\omega = 2\pi f = 2kU_\infty/C$, f is the pitch frequency, ρ is the density of water, U_∞ is the incoming velocity at infinity, C is the hydrofoil chord length, and μ is the liquid viscosity. The coefficients of the lift, drag force, and moment are defined as follows:

$$C_L = \frac{2\mathrm{F}_L}{\rho U_\infty^2 C^2} \tag{5}$$

$$C_D = \frac{2\mathrm{F}_D}{\rho U_\infty^2 C^2} \tag{6}$$

$$C_M = \frac{2M}{\rho U_\infty^2 C^2} \tag{7}$$

where F_L is the hydrofoil lift, F_D is the hydrofoil drag, and M is the pitch moment. The cavitation number is defined as follows:

$$\sigma = \frac{p_\infty - p_v}{0.5\rho U_\infty^2} \tag{8}$$

where p_∞ is the pressure of incoming flow and p_v is the saturated vapor pressure of water.

2.2 Numerical method and validation

The domain utilized for computation is illustrated in Fig. 1. A NACA 0012 hydrofoil was chosen as the object of interest. A structured mesh was created using the specialized software of ICEM CFD, and a local refinement technique was employed in the vicinity of both the free surface and the hydrofoil to ensure that the nondimensional wall distance, denoted by y+, was kept below unity (i.e., y+ < 1).

The present study employs the ANSYS Fluent software based on the finite volume method to simulate the unsteady and incompressible cavitation flow of an oscillating hydrofoil with a free surface. The hydrofoil's pitching is adjusted by a user defined function to control its oscillatory motion, while the sliding mesh interpolation technique is employed to facilitate data exchange between the moving and stationary domains. The inlet boundary condition is given by the open channel with prescribed flow velocity and water depth, and the outlet is set as a static pressure boundary. The hydrofoil surface is treated as a no-slip wall. The study considers two working conditions, namely, light cavitation and deep cavitation, with the calculation parameters presented in Table 1. A coupled algorithm based on pressure is adopted to solve the governing equations synchronously with second order spatial-time discretization [24]. The VOF model is used to simulate the near-free surface flow, while the Schnerr-Sauer cavitation model and the SST k-ω turbulence model are used to simulate the phase change and turbulent motion, respectively.

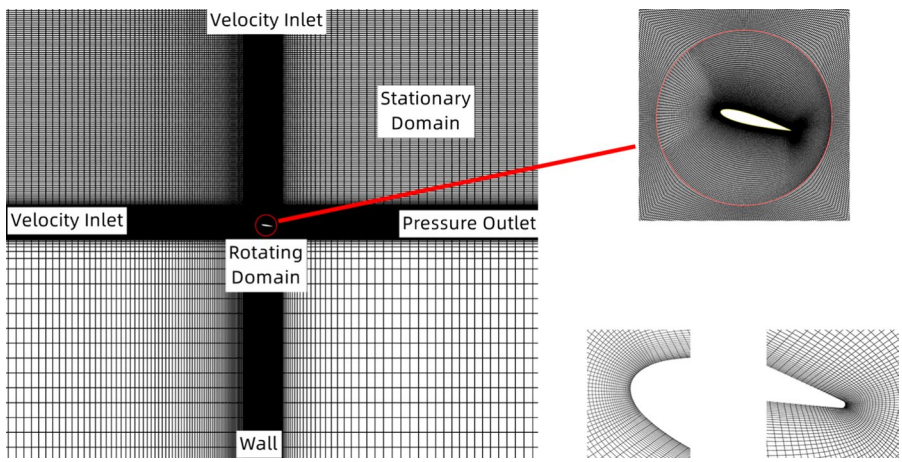

Fig. 1 Compute domains and boundary conditions

In this study, we present the sensitivity analysis of mesh resolution and time step using the operating condition of case VI. Regarding the mesh resolution analysis, we maintained the grid points number of 39,026 in the station domain consistently across all three sets of grids. However, for the rotating domain, as indicated in Table 2, we varied the grid points number in both the circumferential and radial directions while ensuring that all hydrofoil wall y+ values remained below 1. Figure 2a illustrates that the hysteresis curves of Grid2 and Grid3 overlap more closely as the mesh density increases. Additionally,

Table 1 Computational parameters

Stall type	Light stall			Deep stall			Exp.	
Cases	I	II	III	IV	V	VI	①	②
$\overline{\alpha}$(°)	-2	15	15	15	15	15	15	7.5
A (°)	10	10	10	10	10	10	10	7.5
Re	5×10^6	2.5×10^6	2.5×10^6	2.5×10^6	2.5×10^6	2.5×10^6	1×10^6	7.5×10^6
k	0.1	0.15	0.05	0.15	0.15	0.15	0.15	0.02
σ	0.5	0.5	0.5	1.0	1.3	0.1	–	8.0
ω	1	3	1	3	3	3	0.6	1.26
$ds=d/C$	1	2	2	2	4	1	–	–

Table 2 Mesh distribution in rotating domain

Case number	Number of grid points in circumferential direction	Number of grid points in radical direction	Aspect ratio from the hydrofoil wall	Number of grid points in rotating domain
Grid1	320	130	1.15	40,764
Grid2	370	170	1.10	61,854
Grid3	420	200	1.05	82,784

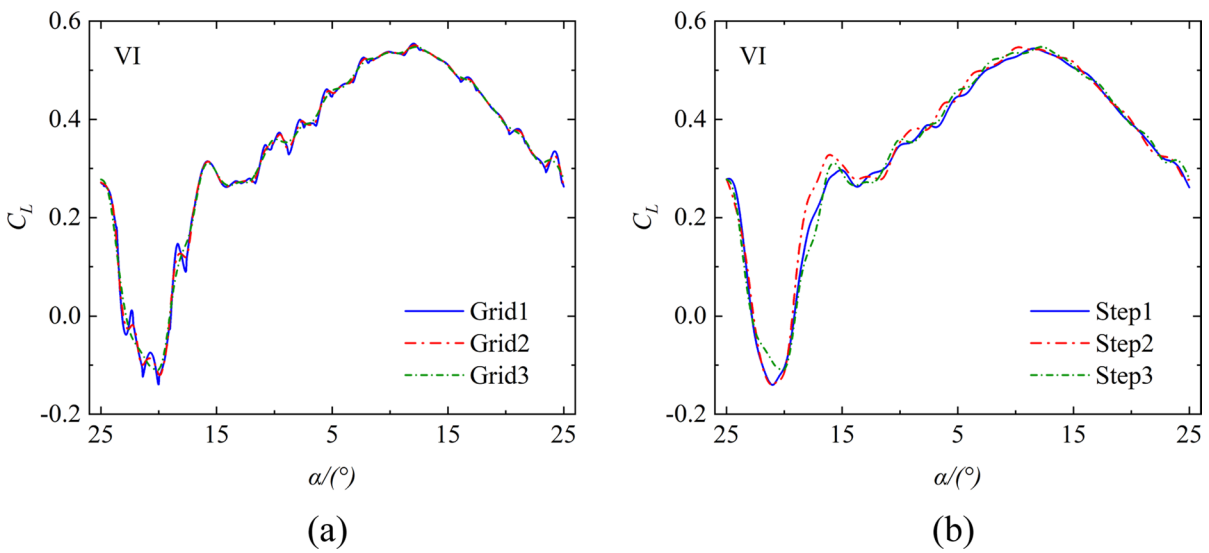

Fig. 2 Sensitivity study of grid resolution and time step (Case VI; Grid1:40,764, Grid2:61,854, Grid3:82,784; Step1 = 0.002 s, Step2 = 0.0015 s; Step3 = 0.001 s)

from Fig. 2b, it is evident that using the smallest time step results in more oscillations in the curve, indicating that reducing the time step enables a more accurate capture of the cavity shedding process. Based on the previous simulation experience [25, 26], in this study, the mesh with total number of grid points of 121,810 and a time step of 0.001 s were carefully chosen to ensure the accurate simulation of the cavitation flow field near the free-surface. A stable convergence solution can be obtained after at least 10 oscillation cycles of the hydrofoil, and the flow field of the last cycle is analyzed for subsequent results.

To evaluate the accuracy of the calculation method, we compare simulation results of the oscillating hydrofoil under deep stall conditions with experimental data, both with and without cavitation generation. As shown in Fig. 3a, we compare the lift coefficient of the NACA 0012 oscillating hydrofoil in the non-cavitating flow field with experimental data ① [27, 28]. We observe that during the hydrofoil's upstroke phase in deep stall conditions, the lift coefficient increases with the increase of attack angle. However, when the oscillating hydrofoil returns after reaching its maximum angle of attack, the lift coefficient drops sharply due to the delay effect caused by dynamic stall of the oscillating hydrofoil, and the fluctuation amplitude is large. In Fig. 3b, we also compare the lift coefficient of the NACA 66 oscillating hydrofoil with $\sigma = 8.0$ and the experimental data ② [16]. Overall, our numerical simulation results agree well with the experimental results, demonstrating the feasibility of the currently employed calculation method.

We also conducted a numerical simulation using a NACA0012 hydrofoil in a static water condition as an example [29]. The Reynolds number was $Re = 1.62 \times 10^5$, the Froude number was $Fr = 0.577$, the hydrofoil angle of attack was 5°, and the immersion depth (ds = d/C) was 0.95. In Fig. 4, we compare the numerical simulation with experimental results

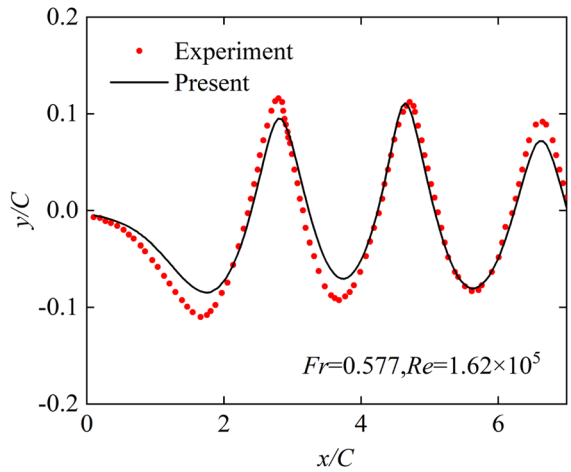

Fig. 4 Comparison of calculated free surface shape of a static hydrofoil with test data

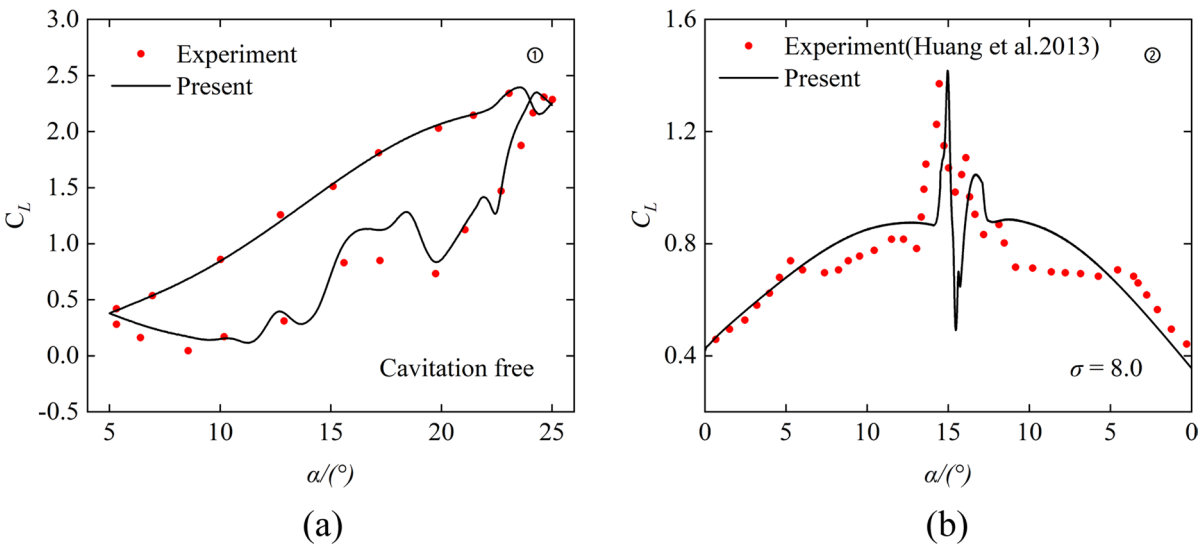

Fig. 3 Comparisons of lift coefficient in deep stall condition, **a** cavitation free, **b** $\sigma = 8.0$

and find that the free surface shapes of both methods are basically identical. This comparison supports the feasibility of our free surface simulation and boundary condition treatment method.

3 Results and discussions

Table 1 presents a summary of the calculated parameters for oscillating hydrofoils with free surface effects, under various stall conditions. The primary focus of this study is on the occurrence of cavitation for hydrofoils experiencing both light and deep stall conditions. Additionally, the impact of various reduced frequencies (k), cavitation numbers (σ), and immersion depths (ds) on the hysteresis curve under deep stall conditions are investigated.

Figure 5 depicts the overall distribution of cavitation volume fraction near the free surface for oscillating hydrofoils experiencing light stall conditions. The figure reveals that the oscillating hydrofoil induces waves on the free surface, which, in turn, affects the evolution of the hydrofoil's cavitation flow field. The detailed effects will be discussed in Sect. 3.3.

3.1 Light stall

To investigate the impact of cavitation on the hysteresis effect of the oscillating hydrofoil's force and moment coefficients during light stall conditions, a comparative analysis was performed based on the computational parameters of Case I outlined in Table 1. As shown in Fig. 6, the occurrence of cavitation significantly amplified the hysteresis

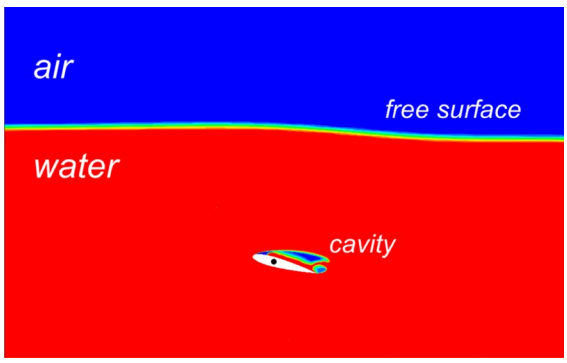

Fig. 5 Cavitation flow fields of an oscillating hydrofoil near free surface

effect of the hydrofoil's performance parameters, particularly at large angles of attack, where the presence and evolution of cavitation induced significant fluctuations in the performance parameters. Moreover, the effect of cavitation-induced hysteresis was more prominent at large negative angles of attack. Figure 6a shows that, when compared with the cavitation-free case, the amplitude of the C_L for the hydrofoil pitching up (with abbreviated letter u in the figure) from a large negative angle of attack was smaller in the presence of cavitation. The amplitude then increased to approximately the same as the cavitation-free case at low angles of attack, and finally surpassed the cavitation-free case at large angles of attack. When the hydrofoil was pitching down, the amplitude of the C_L was initially greater than the cavitation-free case, then decreased below the cavitation-free case at low angles of attack, and ultimately became smaller than the cavitation-free case at large negative angles of attack. Additionally, Fig. 6b, c revealed that, except for the cavitation-free hydrofoil's C_D and C_M, which remained relatively constant in the vicinity of low angles of attack, the occurrence of cavitation substantially increased the hydrofoil's drag coefficient and moment coefficient relative to the oscillation center within the range of large positive and negative angles of attack.

Figure 7 shows the volumetric distribution of cavitation on the surface of the oscillating hydrofoil during light stall conditions. At a large positive angle of attack, cavitation appears on the upper surface of the hydrofoil, and the cavitation intensity during the upstroke is notably stronger than during the downstroke. In contrast, at a large negative angle of attack, cavitation arises near the leading edge on the lower surface of the hydrofoil, and the cavitation intensity during the downstroke is significantly stronger than during the upstroke. This disparity in cavitation intensity at the same angle of attack further amplifies the hysteresis effect of the hydrofoil performance curve.

Figure 8 presents a comparison of vorticity contours near the hydrofoil surface during light stall conditions, with and without cavitation generation. The results indicate that, under cavitation-free conditions, attached vortices cover the hydrofoil surface. However, when cavitation arises at high angles of attack, the vorticity predominantly concentrates near the strong shear layers at the interface between the two

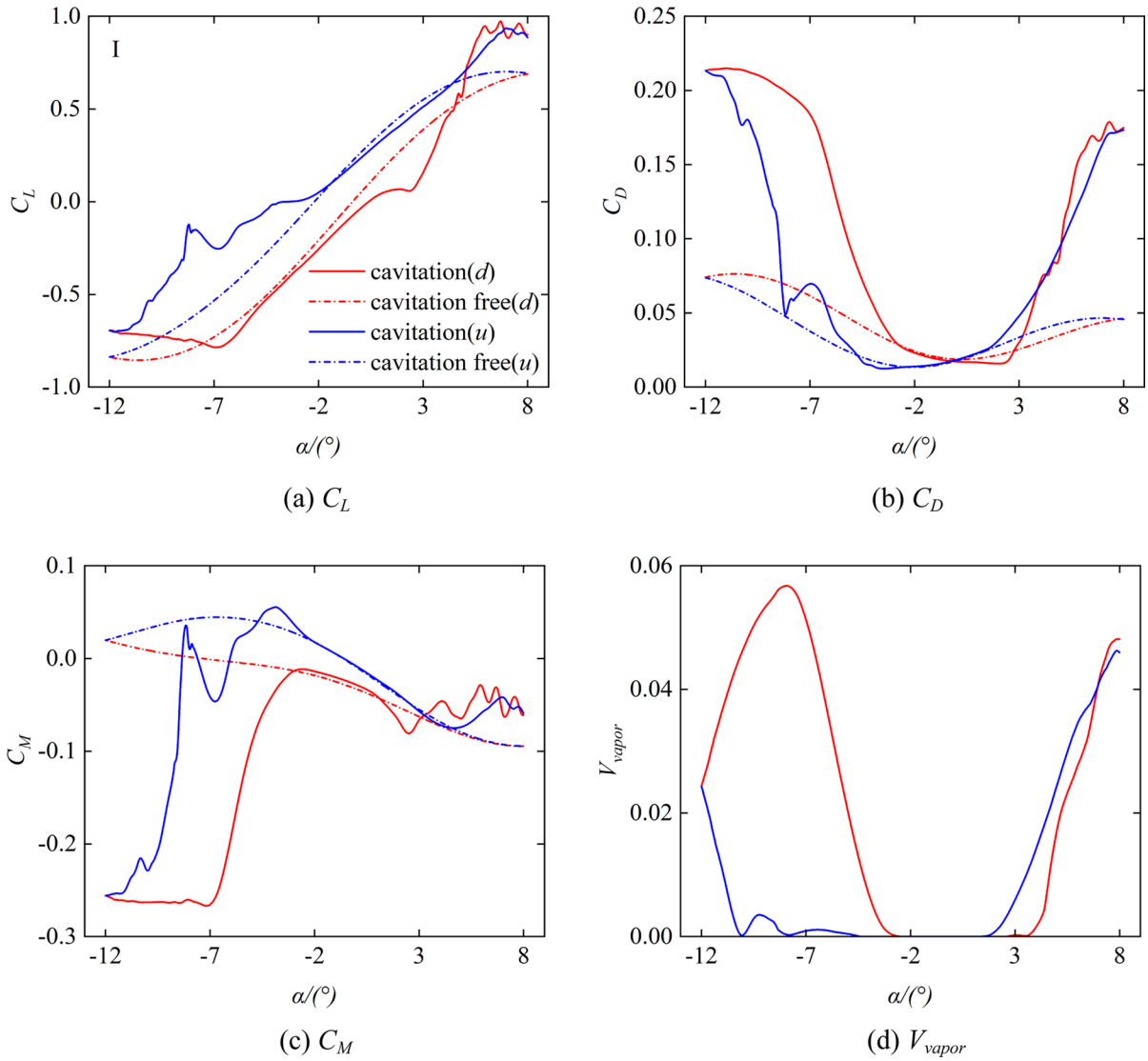

Fig. 6 Comparisons of performance hysteresis at the light stall condition

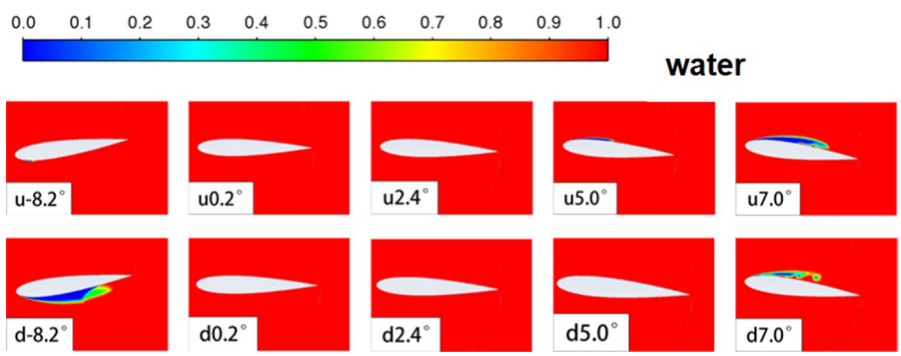

Fig. 7 Vapor volume fraction in light stall condition

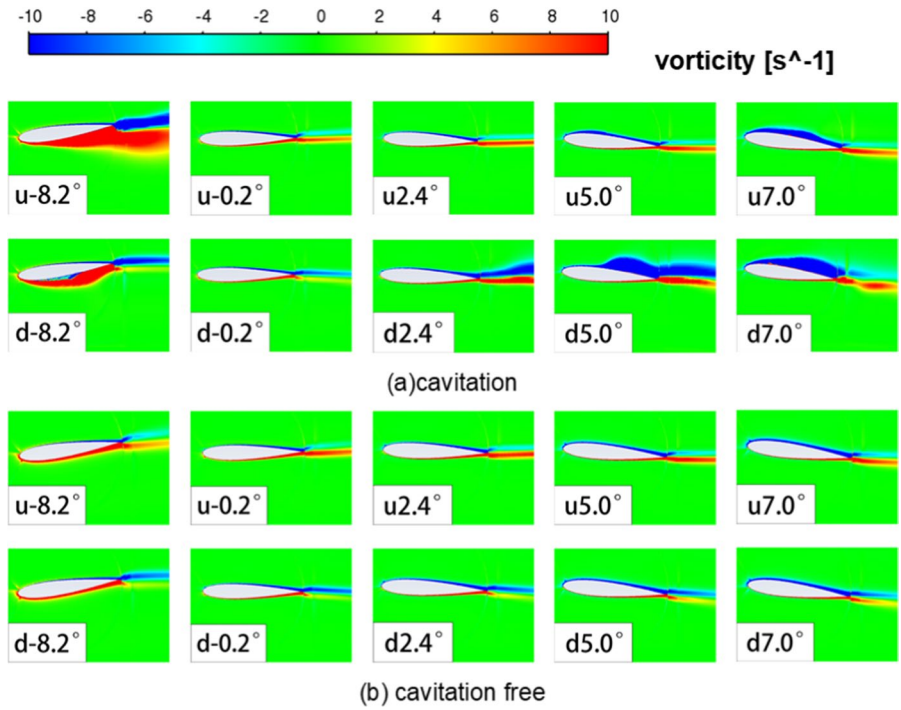

Fig. 8 Comparisons of vorticity distribution in light stall condition

phases. This leads to a notable asymmetry in the distribution of vorticity.

3.2 Deep stall

The impact of cavitation was evaluated for the deep stall state at Case II, as presented in Table 1. As illustrated in Fig. 9, the performance hysteresis curves demonstrate significant overlap when the α is small, and cavitation effects are absent. However, as α increases, the difference in force coefficient variations between cases with and without cavitation becomes more pronounced, especially as cavitation in the flow field intensifies. When cavitation occurs, the hysteresis loops of the performance curves display more fluctuations, but the overall numerical shift is smaller. In the absence of cavitation, the force coefficient curve during the upstroke process is smooth, with minor numerical shifts, whereas the force coefficient during the downstroke process exhibits prominent peaks with a larger range of numerical changes. Figure 9a shows that cavitation occurrence reduces the C_L of the hydrofoil at high angles of attack. Additionally, Fig. 9b indicates that under the condition of cavitation occurring, the C_D of the hydrofoil exhibits a fluctuating upward trend as the stall angle increases, and its average of C_D at high angles of attack is higher than that without cavitation. Furthermore, under cavitation-free conditions, the C_D experiences a sudden increase during the downstroke process of the hydrofoil when the attack angle is within the range of 15°–21°. Figure 9c reveals that under cavitation occurring conditions, the C_M remains relatively stable. However, in the cavitation-free scenario, multiple peaks with significant numerical changes are observed during the downstroke process, and these peaks occur in the corresponding angle of attack range of 15°–21°, demonstrating pronounced hysteresis.

Figure 10 reveals that the hydrofoil experiences a gradual increase in cavitation volume fraction during the upstroke phase, starting from attached cavitation at low angles of attack and transitioning into a detached cloud cavitation state dominated by large backflow at high α. Conversely, during the downstroke phase, there is a significant phase difference in the cavitation volume evolution compared to the upstroke, and the intensity of cavitation occurrence is reduced, as supported by the quantitative statistics displayed in Fig. 9d. At high angles of attack, the increased strength of the vortex cavitation reduces the C_L.

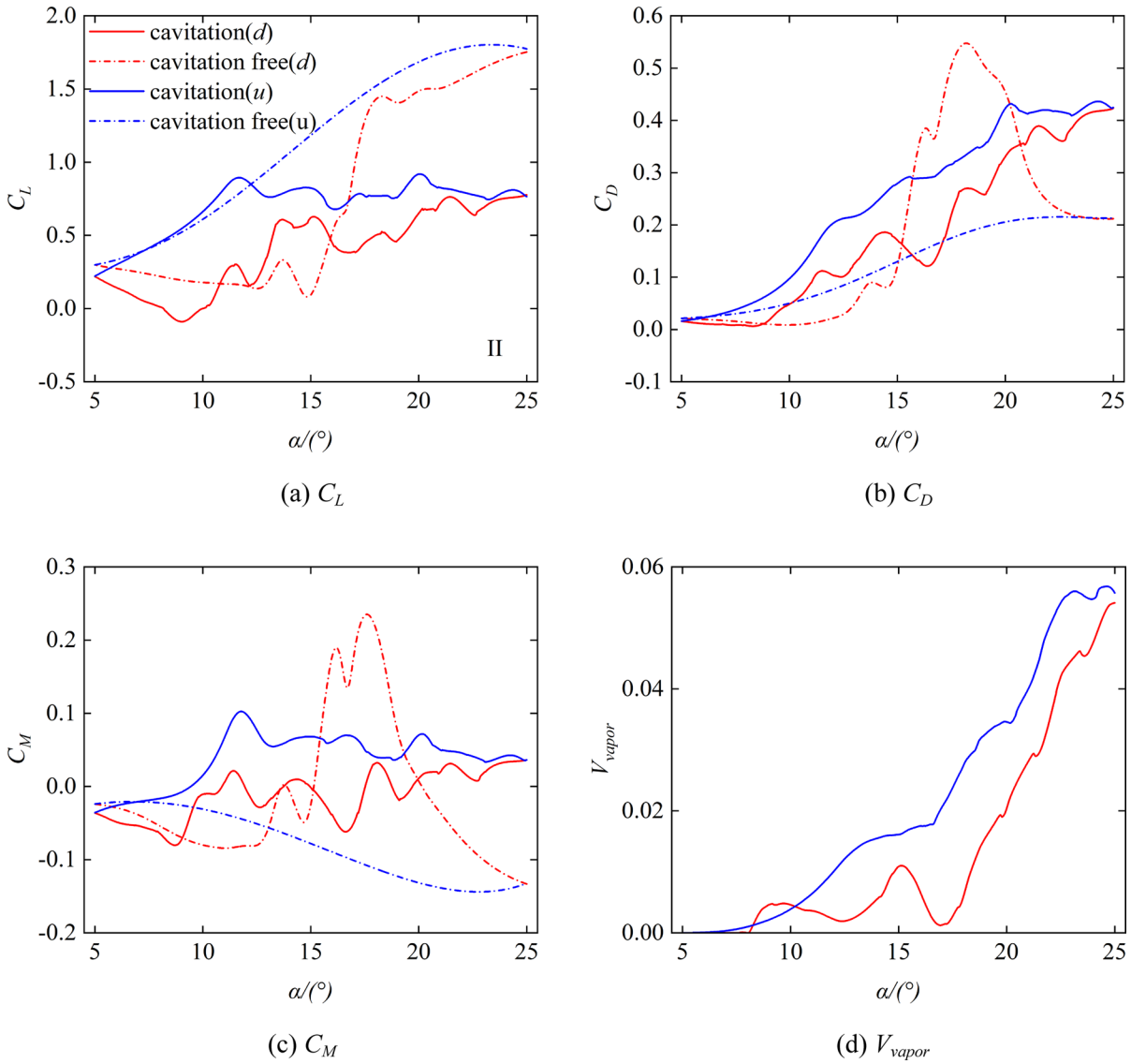

Fig. 9 Comparisons of performance hysteresis in deep stall conditions

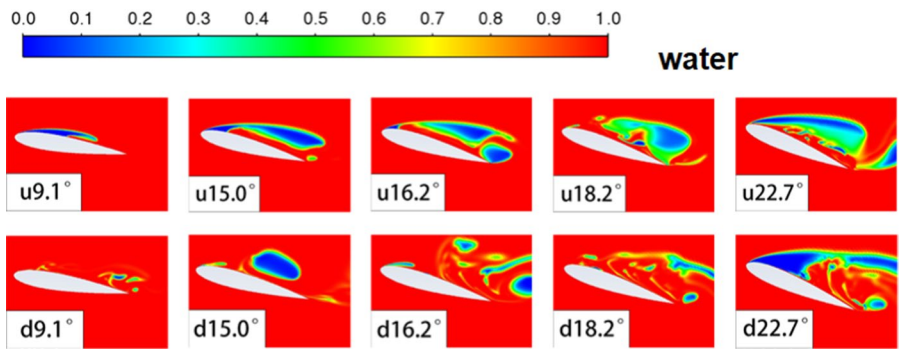

Fig. 10 Water vapor fraction in deep stall conditions

Figure 11 presents a comparison of the vorticity distribution, indicating that flow separations occur on the upper surface of the hydrofoil due to the positive angle of attack in the investigated deep stall condition, while attached vortices dominate the lower surface. Cavitation causes the vorticity to concentrate primarily at the two-phase interface. Under the cavitation-free condition during the upstroke phase, there is no apparent vortex separation on the hydrofoil's upper surface, whereas the vortex structure on the upper surface fluctuates periodically with the development of cavitation clouds and the angle of attack under cavitation conditions, which explains the fluctuating performance parameters and non-smooth performance curve of the hydrofoil. During the downstroke phase, the vorticity near the hydrofoil exhibits distinct characteristics that differ from the upstroke phase, particularly under the cavitation-free condition. After reaching the maximum value during the upstroke phase, a large separation vortex is induced at the leading and trailing edges of the hydrofoil and then evolves along the surface of the hydrofoil. As the angle of attack decreases, the separation vortex gradually weakens and approaches that of the upstroke phase under the same angle of attack. These differences are the primary reasons for the variations in the formation and existence of the hysteresis curves under cavitation and cavitation-free conditions.

3.2.1 *Effects of reduced frequency k*

To demonstrate the effects of reduced frequency on the hysteresis curve of an oscillating hydrofoil, Case III was established by adjusting the reduced frequency to $k = 0.05$ based on Case II. Figure 12 shows the force coefficients of Cases II and III. Overall, as the reduced frequency k decreases, the hysteresis curve of the hydrofoil fluctuates more significantly, while having a negligible impact on the numerical value range. From Figs. 12d and 13, it is evident that the severity of volume fraction fluctuation increases with reduced frequency, indicating periodic cavitation development along the hydrofoil surface during low-frequency oscillation, which explains the pronounced fluctuation of the oscillating hydrofoil's hysteresis curve. Furthermore, low-frequency oscillation substantially reduces cavitation intensity, with similar intensities during both the upstroke and downstroke.

To investigate the flow field differences at the corresponding angles of attack where hysteresis curve discrepancies exist between two test cases, the vorticity distribution is analyzed and compared in Fig. 14 for different reduced frequencies. The results show

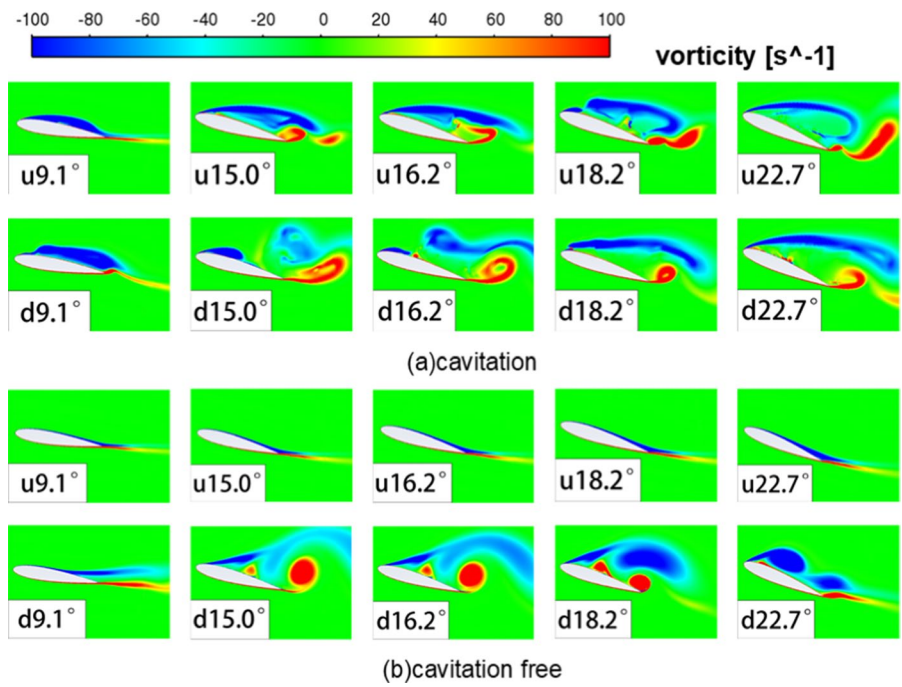

Fig. 11 Comparison of vorticity distributions in deep stall conditions

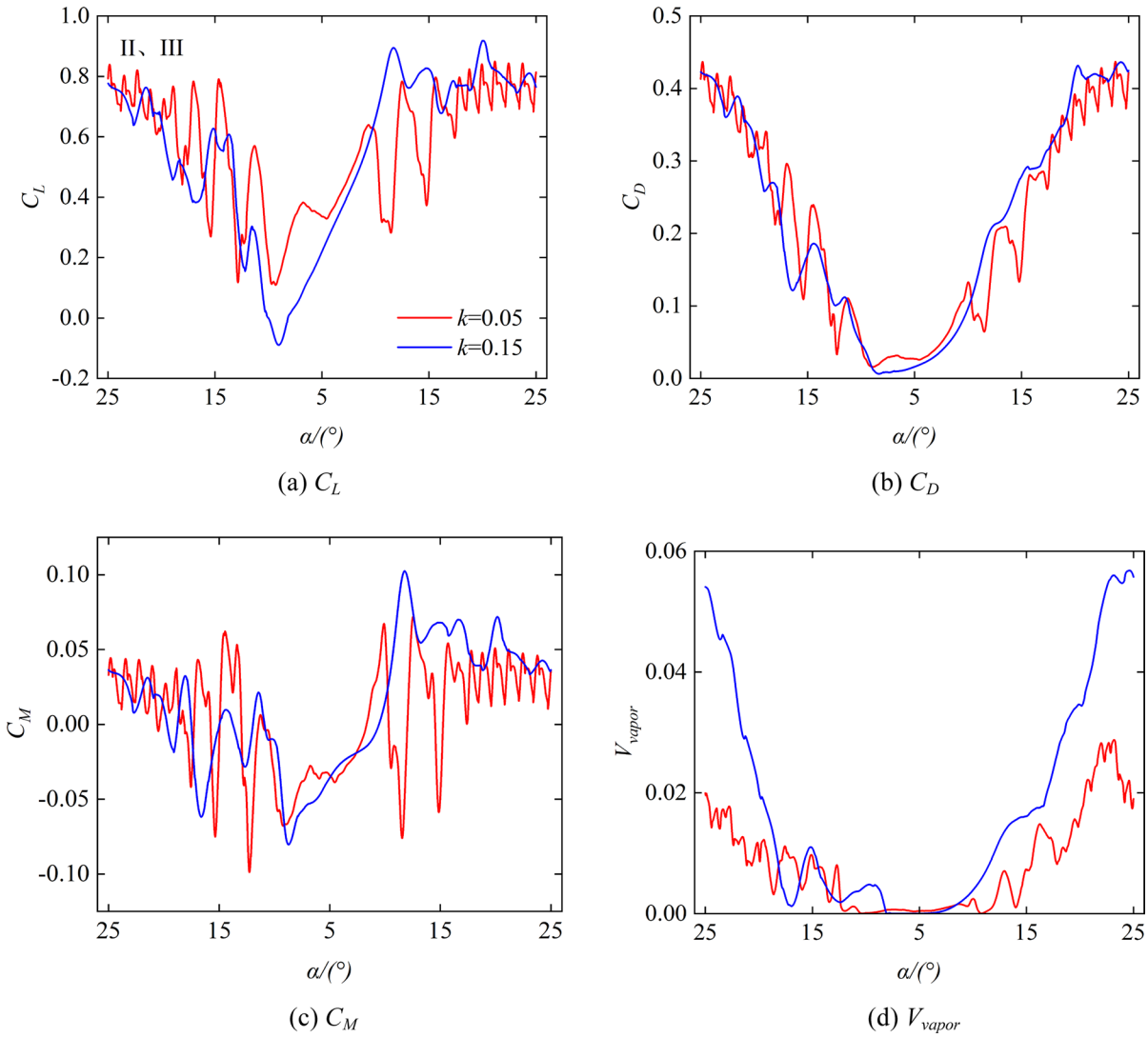

Fig. 12 Effects of reduction frequency k on hysteresis performance

that the variation of reduced frequency significantly impacts the evolution period of vortical structures on the upper surface of the hydrofoil, while the variation in vorticity magnitude is relatively minor. Particularly at high α near the stall condition, the separation frequency of vortical structures at the trailing edge in the case of $k=0.05$ is substantially higher. This accounts for the performance curve fluctuations, although the numerical variation range remains largely unchanged. In the case of $k=0.05$, the vorticity distribution of the hydrofoil at the same α during pitch motion is essentially identical, resulting in minimal differences in force coefficients at these α. However, in the case of $k=0.15$, the hysteresis effect on the curve is evident, leading to notable differences in the vorticity distribution during pitch motion.

To investigate the underlying mechanism of the low-frequency hysteresis curve fluctuations, this study conducted pressure measurements at ten points on the hydrofoil's backpressure surface, ranging from the leading edge to the trailing edge. As shown in Fig. 15, the pressure coefficient difference at various positions is primarily evident in areas with smaller angles of attack, with the pressure coefficient increasing towards the trailing edge for the condition of $k=0.15$. This trend is mainly attributed

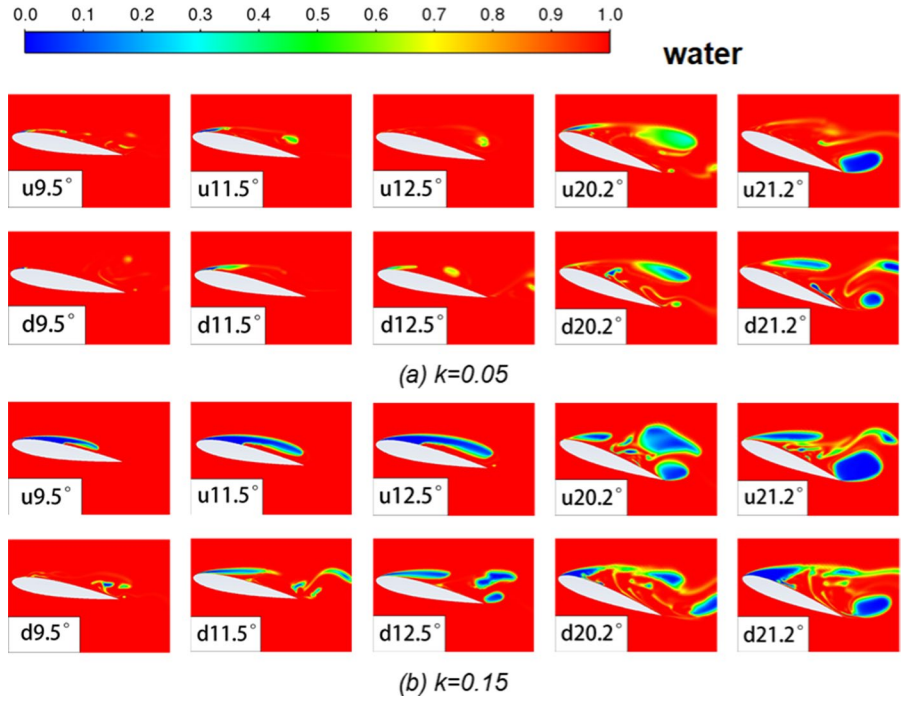

Fig. 13 Comparisons of water vapor volume fraction at different reduction frequencies

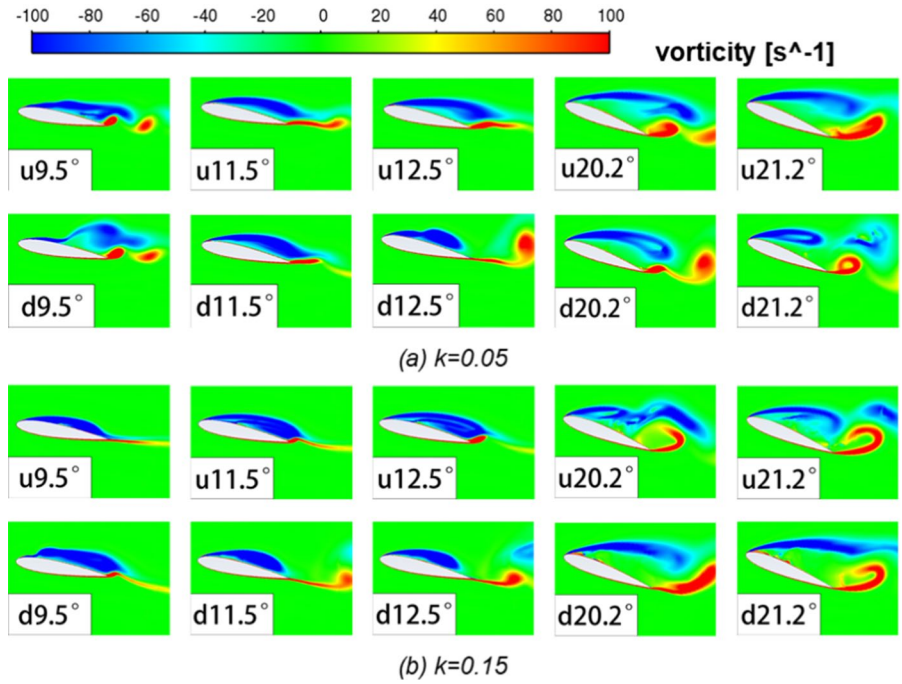

Fig. 14 Comparisons of vorticity distribution at different reduction frequencies

to the formation of cavities caused by the incoming flow at the leading edge, leading to a local reduction in pressure. Regarding the pressure distribution at a specific position, the pressure on the backpressure surface attains its maximum value at approximately $\alpha = 17°$, and the pressure peak during the downstroke process exceeds that of the upstroke process. As the pressure peak generated during the upstroke process

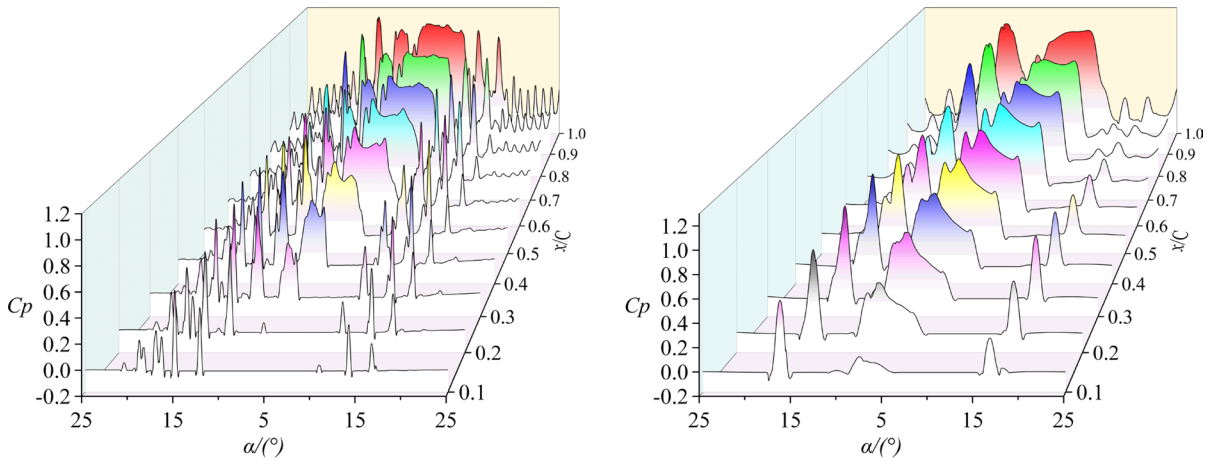

Fig. 15 Comparison of pressure coefficient variation at different positions on the back pressure surface of oscillating hydrofoil

gradually decreases towards the trailing edge of the hydrofoil, and the pressure peak generated during the downstroke process gradually increases, the difference between the two peaks becomes more prominent as it approaches the trailing edge. For the condition of $k=0.05$, no pressure fluctuation occurred at the hydrofoil's leading edge at low α, indicating that cavitation took place at the leading edge and did not result in cavity detachment and pressure fluctuations. During the downstroke process at $\alpha>15°$, significant pressure fluctuations occur near the trailing edge of the hydrofoil due to the detachment and collapse of cavities above the backpressure surface of the hydrofoil caused by high angles of attack. Combining the cavitation evolution in the flow field as shown in Fig. 14, it can be concluded that when the reduced frequency is high, a considerable cavity is generated at the hydrofoil's leading edge, which collapses near $\alpha=15°$ and mainly produces a single peak on the upstream side of the backpressure surface. In contrast, when the frequency is low, the hydrofoil generates numerous small cavities, and their collapse mainly occurs at the trailing edge of the hydrofoil, resulting in multiple pressure peaks, which are the primary reason for the oscillation in the hysteresis curve.

3.2.2 *Effects of cavitation number α*

Keeping Fr number as a constant, we change the environmental pressure to alter the cavitation number. Based on Case II with $\sigma=0.5$, Case IV sets the cavitation number of the oscillating hydrofoil to $\sigma=1.0$. Figure 16 shows a comparison of the force coefficients between the two cases. Overall, the trend in the force coefficients with respect to the stall angle is consistent, but the hysteresis curve of Case IV with $\sigma=1.0$ exhibits larger fluctuations and more peaks. As shown in Fig. 16a, at lower α, the hysteresis curves of the two conditions are similar, but as α increases, Case IV with $\sigma=1.0$ begins to exhibit alternating peak-trough changes. Figure 16b shows that, at lower angles of attack, the C_D of Case IV with $\sigma=1.0$ is relatively small, but as α increases, its hysteresis curve exhibits a peak value larger than that of Case II with $\sigma=0.5$. Figure 16c shows that, at lower α, the C_M curve of Case IV with $\sigma=1.0$ is smooth and has a relatively small value. As α increases, the fluctuation of the C_M curve of this condition increases, and the value is relatively large. In the initial stage of the downstroke motion, the C_M curves of both cases exhibit a phase-alternating change with the variation of α. Figures 16d and 17 demonstrate that a decrease in σ leads to an increase in the cavity volume on the surface of the oscillating hydrofoil. In Case IV with $\sigma=1.0$, the volume fraction exhibits a development trend of decreasing first and then increasing in the range of $\alpha=20°$–$25°$, indicating a process of contraction, collapse, and regrowth of the cavity structure in this range.

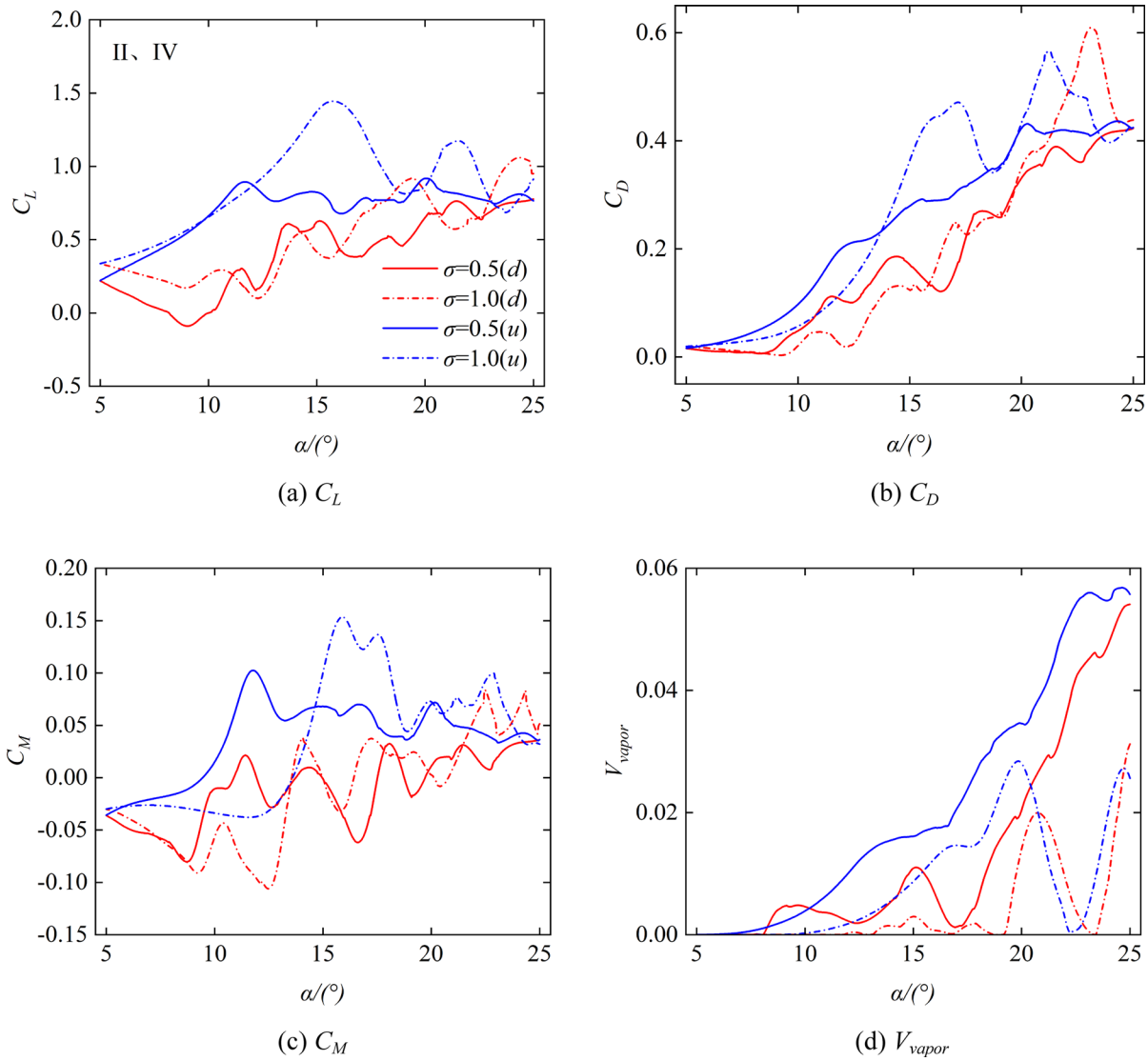

Fig. 16 Effect of cavitation number on hysteresis curve

From the comparison of vorticity distribution under different cavitation numbers in Fig. 18, it can be seen that the change of cavitation number has a significant influence on the vortex shedding pattern on the hydrofoil suction surface. When the hydrofoil is in an upstroke motion, the leading and trailing edge vortices of the case of $\sigma = 0.5$ mainly shed in a strip-like pattern, which has less impact on the hydrofoil force. On the other hand, for the case of $\sigma = 1.0$, the leading-edge vortex attaches to the hydrofoil's suction surface and develops towards the trailing edge as the angle of attack increases. The vortex shedding has a greater impact on the hydrofoil force, which is also the reason for the peak value of the lift coefficient for the case of $\sigma = 1.0$ during the upstroke motion. When the hydrofoil is in a downstroke motion, the leading-edge vortex for the case of $\sigma = 1.0$ no longer attaches to the hydrofoil suction surface, and only differs in vorticity magnitude compared to the case of $\sigma = 0.5$. Therefore, the drag coefficient for the two cases during downstroke motion is approximately the same.

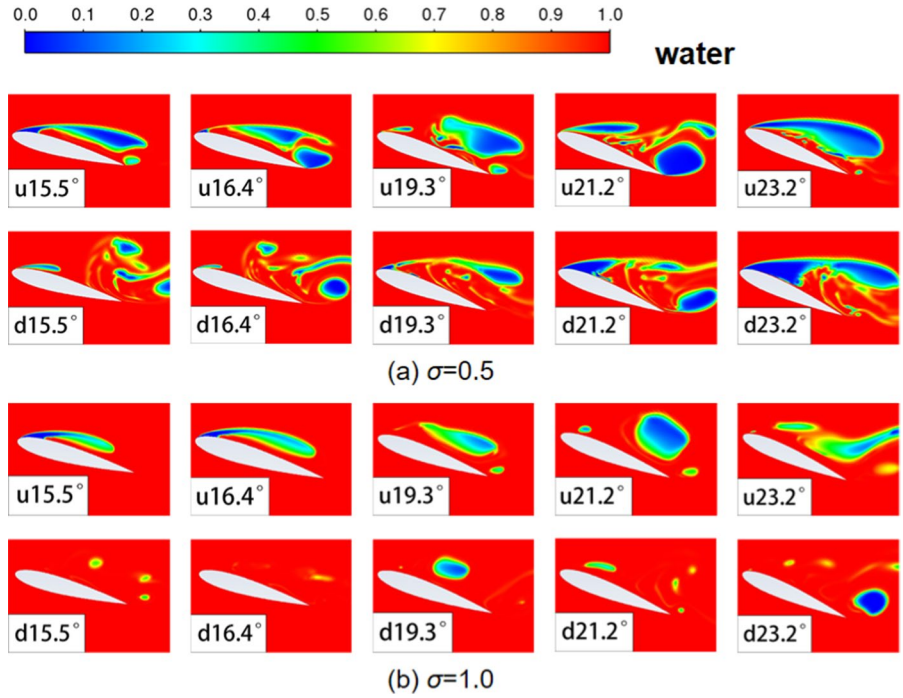

Fig. 17 Comparisons of water vapor volume fraction at different cavitation numbers

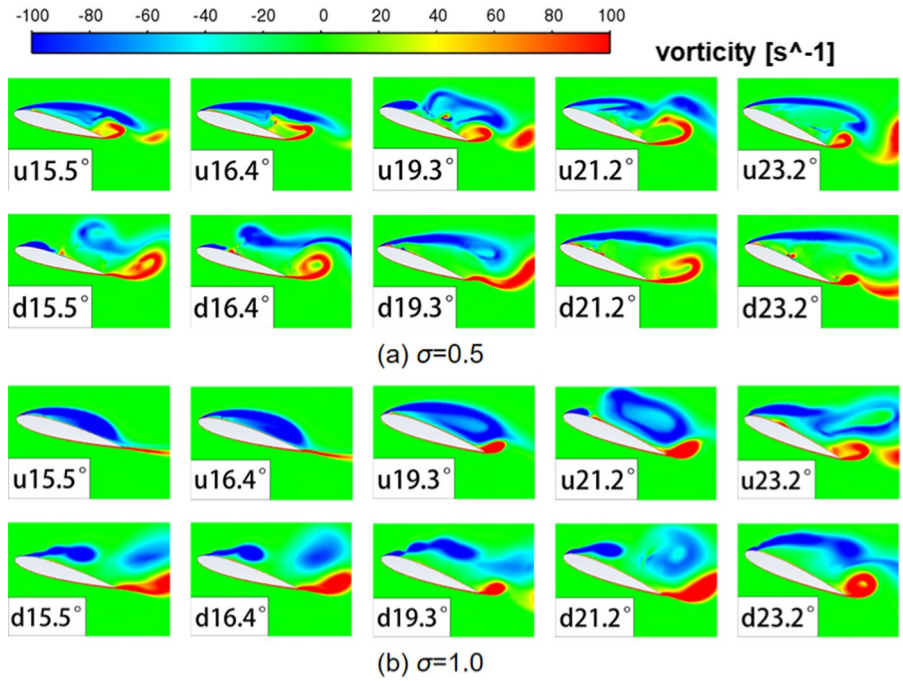

Fig. 18 Comparison of vorticity distributions at different cavitation numbers

3.2.3 Effects of water depth from the free surface

To investigate the influence of different water depths from the free surface on the hysteresis curve of oscillating hydrofoils, two additional operating conditions with $ds=1$ and $ds=4$ were added based on the condition of $ds=2$, and the hysteresis curves of the three conditions were compared in Fig. 19. Overall,

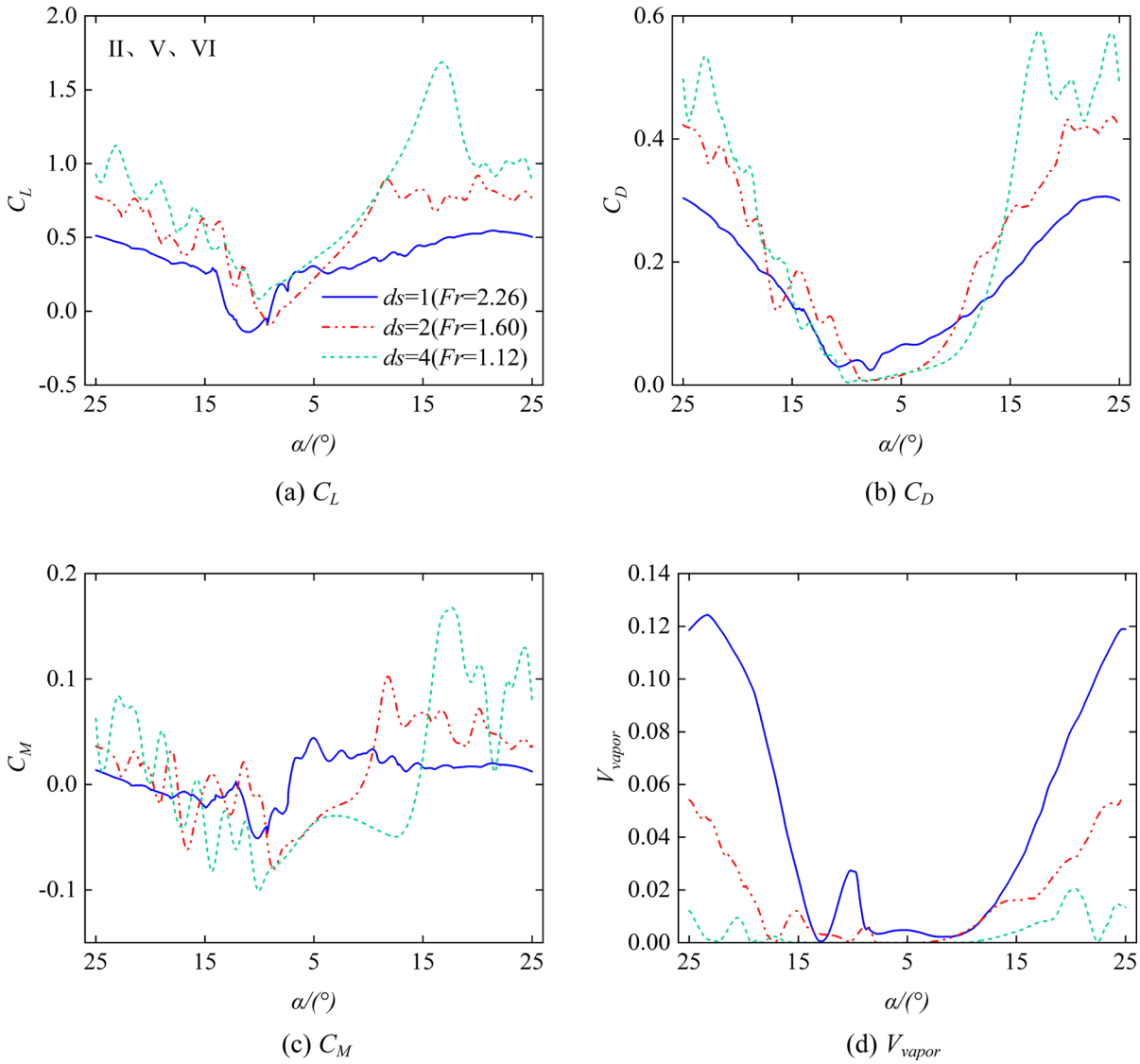

Fig. 19 Effects of water depth from the free surface on hysteresis performance

the variation of the force coefficient is greatly affected by the distance from the free surface, as *ds* decreases, resulting in a significant difference in the region of larger stall angles. As shown in Fig. 19a, a smaller *ds* leads to a lower magnitude and a smaller fluctuation range of the C_L. The variation trend of the C_D in Fig. 19b is similar to that of the C_L, with the only difference being that a smaller *ds* leads to a larger C_D only when $\alpha<10°$, and the C_D exhibits obvious symmetry during the entire pitching motion. In Fig. 19c, a smaller *ds* still leads to a smoother fluctuation of the hysteresis curve, but the fluctuation of the curve during the downward pitching process is quite different from that during the upward pitching process. That is, a larger *ds* leads to a more significant fluctuation of the hysteresis curve, and the fluctuation of the C_M during the downward pitching process is much higher than that during the upward pitching process. By combining Figs. 19d and 20, it can be observed that as *ds* decreases, the cavitation at the region of larger α becomes more severe. When the hydrofoil experiences super cavitation, the pressure on the suction face is equal to p_v. Therefore, the hysteresis curve of $ds=1$ changes smoothly. When *ds* is

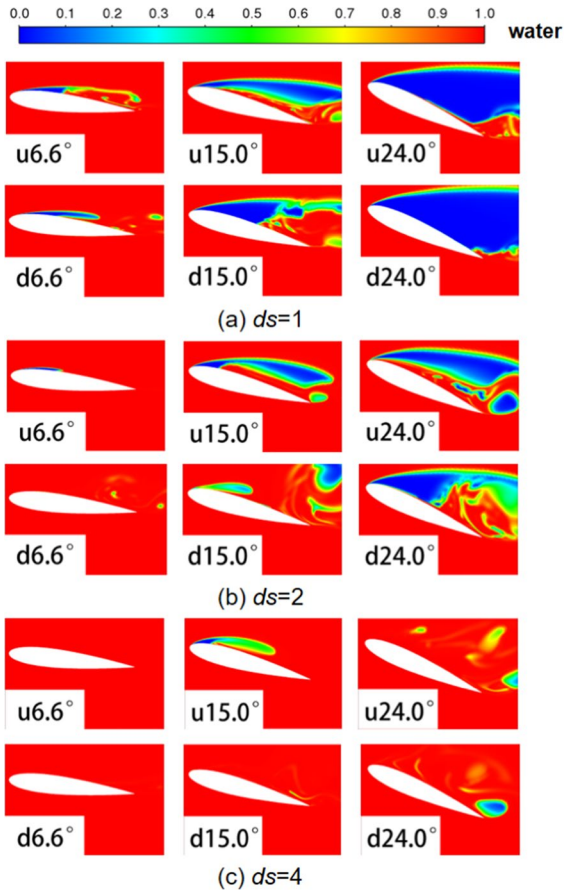

Fig. 20 Comparison of cavitation vapor volume fraction for different *ds*

relatively large, the cavitation on the suction face of the hydrofoil mainly takes the form of small bubbles that frequently detach, especially during the downward pitching process, resulting in a fluctuation of the hysteresis curve. In addition, as shown in Fig. 20d, a peak appears in the volume fraction curve during the downward pitching process of the hydrofoil, which is caused by the detachment of the cavitation on the suction face. As *ds* decreases, the stall angle α of the hydrofoil during the detachment of the cavity becomes smaller, and the volume of the detached cavity becomes larger. These findings indicate that a larger *ds* leads to a more easily suppressed cavitation in the flow field, which affects the detachment type of cavitation bubbles in the flow field, and thus causes a change in the hysteresis curve of the oscillating hydrofoil.

From the comparison of vorticity distribution and velocity streamline with different immersion depths in Fig. 21, it can be seen that the *ds* has a significant influence on the vorticity distribution of the oscillating hydrofoil. As *ds* decreases, vortexes are more likely to form on the hydrofoil's pressure side, especially at α=6.6°, where vortexes are mainly generated by the shedding and collapse of small cavities above the hydrofoil's trailing edge. When the hydrofoil reaches $\alpha = 15°$, a larger cavity volume is formed during the upstroke, which is less likely to shed. On the downstroke, cavities on the pressure side begin to shed. The velocity streamline and volume distribution cloud map show that as *ds* increases, the location where cavities collapse and shed is closer to the trailing edge. As a result, significant vortexes are generated at the trailing edge, leading to significant fluctuations in the lift curve. At $\alpha = 24°$, the hydrofoil is more likely to experience cavitation. At the condition of $ds = 1$, super cavitation forms on the hydrofoil's surface, and almost no vortex shedding occurs inside the cavity. When $ds = 2$, a cloud cavitation structure appears on the hydrofoil's surface, and large cavities shed during the downstroke, forming small vortex structures at the shedding locations. At $ds = 4$, only small cavities shed in the flow field. At this point, significant vortex structures form above the hydrofoil's pressure side, and with the shedding and regeneration of vortex structures, the lift curve shows violent fluctuations, which are more likely to exhibit peak values.

3.3 Effects of the free surface shape

To investigate the impact of hydrofoil's oscillation on the free surface shape, Fig. 22a shows the alterations in the free surface shape at various angles for the hydrofoil during deep stall conditions, wherein a stable and periodic oscillation of the free surface occurs. With the premise of maintaining the position of the free surface, changes in submergence depth were achieved by adjusting the coordinate values of the oscillating hydrofoil at (0, *Y*), where $Y = 2 - d$, and *d* is the distance between the hydrofoil and the free surface. The observations reveal that, under different oscillation angles, the phase of the wave crest and trough above the hydrofoil is essentially identical, whereas the phase of the free surface wave farther from the hydrofoil demonstrates a notable increase.

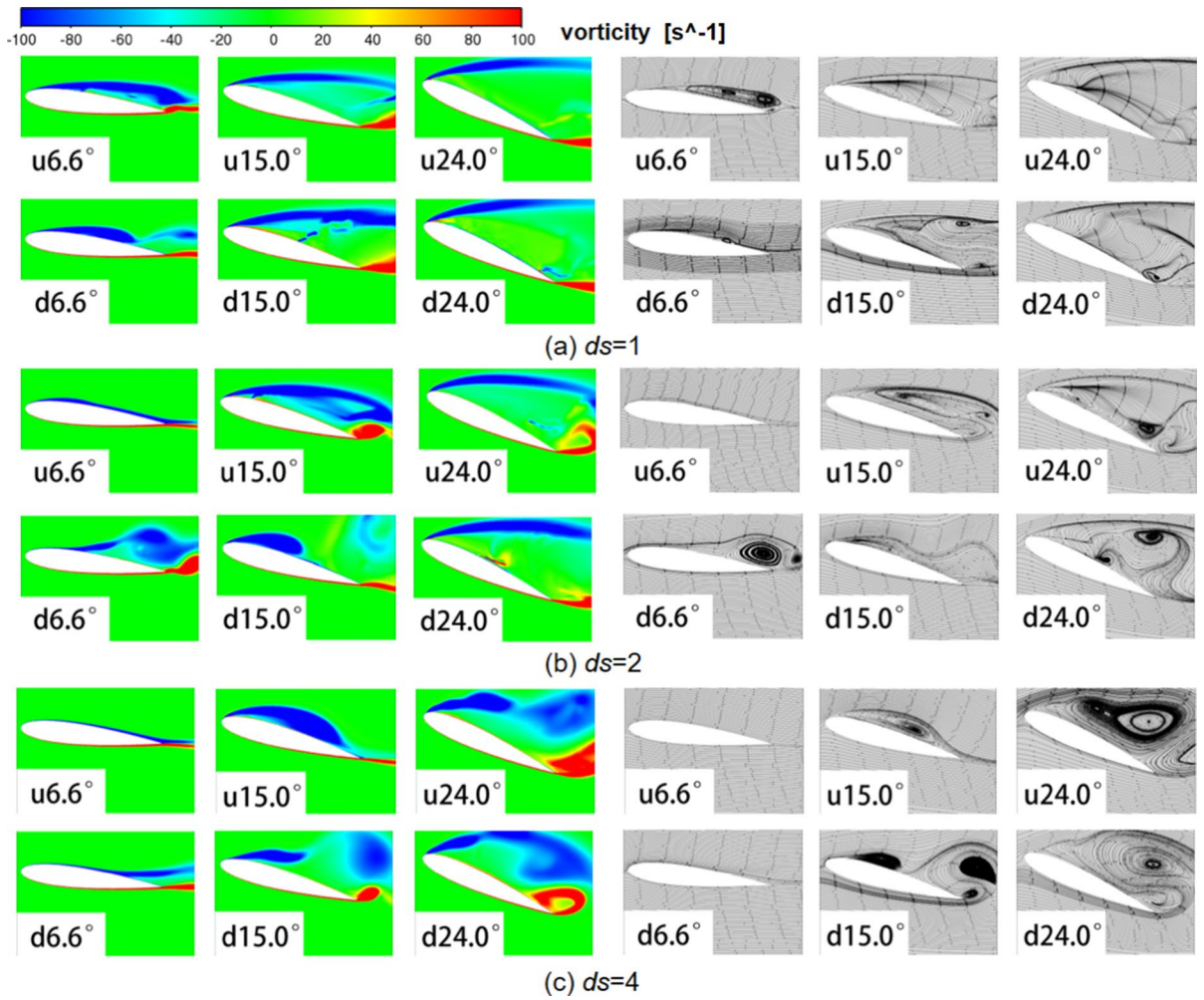

Fig. 21 Comparison of vorticity distribution and velocity streamline for different *ds*

Figure 22b–f present a comparison of the free surface shapes of the oscillating hydrofoil at the mean angle of attack for each operating condition. Figure 22b corresponds to the light stall condition, where the phase of the free surface changes during the pitching motion due to the transition between positive and negative α. When the hydrofoil pitches upward, the α shifts from negative to positive, producing a wave crest on the free surface above the leading edge. Conversely, when the hydrofoil pitches downward, the α shifts from positive to negative, leading to a wave trough on the free surface above the leading edge. The cavitation-free and cavitating generation primarily affect the amplitude of the free surface waves, but have little effect on the trends of the free surface shape. During the pitching up motion, the amplitude of the free surface wave is larger in the cavitation-free condition.

Figure 22c corresponds to the deep stall Case II, where the trend of free surface changes during the upstroke and downstroke is roughly similar, and the amplitude of free surface oscillation is still more significant in the cavitation-free condition. Thus, the occurrence of cavitation in the flow field of the oscillating hydrofoil reduces the amplitude of free surface oscillation, with a larger amplitude during the downstroke. Comparing with Fig. 10, it is evident that the performance curve is smoother during the upstroke, while it fluctuates and peaks during the downstroke. The greater the amplitude of free surface

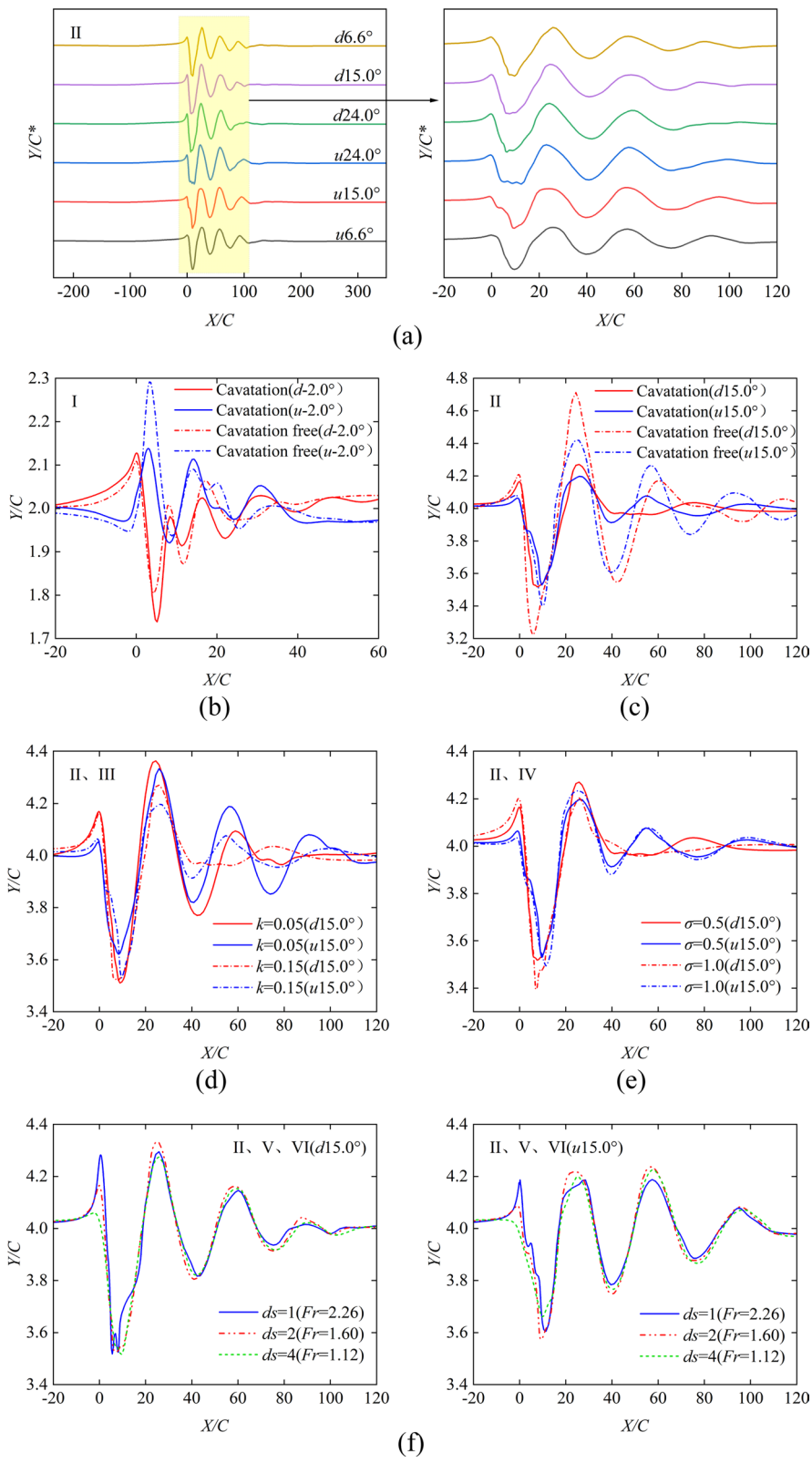

Fig. 22 Comparison of the free surface shape for different working conditions

oscillation, the more significant the fluctuation of the corresponding performance curve. Figure 22d demonstrates that reducing the pitching frequency will increase the amplitude of free surface oscillation, and the hydrofoil's performance curve with a lower pitching frequency in Fig. 12 exhibits a higher oscillation frequency. Figure 22e indicates that varying the cavitation number does not affect the overall shape of the free surface, and the difference in the crest of the free surface primarily affects the magnitude of the hydrofoil performance parameters shown in Fig. 16. Figure 22f illustrates the influence of different values of *ds* on the free surface shape. As *ds* increases, the hydrofoil's effect on the free surface gradually weakens, leading to a decrease in the amplitude of free surface oscillations. Since cavitation is more prone to occur during the downstroke and affects the free surface, the amplitude of free surface oscillation during the downstroke is greater than that during the upstroke.

4 Conclusions

This investigation aims to analyze the hysteresis behavior of the force coefficients and free surface shape of an oscillating hydrofoil under various dynamic stall conditions by means of numerical simulations. The study examines the impact of different parameters on the hydrofoil's behavior, including the stall attack angle (α), reduced frequency (k), cavitation number (σ), and immersion depth (ds). The hysteresis behavior at the same angle of attack under different conditions is investigated, and the causes of the differences are analyzed. The main findings of this study are as follows:

(1) Cavitation significantly affects the variability of the hysteresis curve. This influence can be mitigated through the reduction of the stall angle, along with an increase in the reduced frequency, cavitation number, or water depth from the free surface. As the stall angle increases, the distinction in hysteresis performance becomes more evident, accompanied by a corresponding increase in cavitation intensity. A reduction in the reduced frequency can significantly enhance the oscillation of the force coefficient, whereas alterations to the remaining factors have a relatively minor effect on the performance hysteresis when the attack angle is small.
(2) Cavitation bubble collapse and shedding can lead to short-term, local high pressure on the hydrofoil's suction side, causing fluctuations in the pressure coefficient, especially near the trailing edge of the hydrofoil. Smaller cavities collapsing often leads to more significant fluctuations in the pressure coefficient than larger one's shedding. Hence, when many small cavities are present above the hydrofoil suction surface, the trailing edge experiences severe pressure fluctuations, and the hysteresis curve exhibits noticeable oscillations. The changes in the hysteresis curve tend to appear smoother at smaller angles of attack or when the cavitation phenomenon is not considered.
(3) The evolution and separation of vortices lead to changes in the lift and drag coefficients, with vortex shedding becoming more pronounced during deep stall conditions. In conditions where cavitation is weak, the block vortex structure primarily evolves along the wall, detaches at the mid-chord length, and subsequently migrates downstream. Conversely, in conditions where cavitation is prominent, the vortex evolves mainly from the leading edge to the trailing edge in the form of an elongated strip. During the evolution of the attached block vortex structure along the wall, the lift and drag coefficients exhibit smoother trends before shedding, and they display more prominent peaks during vortex shedding. In situations where the vortex assumes a long strip-like shape, the lift and drag coefficients experience strong fluctuations. However, the overall range of oscillation remains small due to the significant distance from the wall.
(4) The presence of a free surface has a significant impact on the cavitation flow field surrounding a hydrofoil. The proximity of the hydrofoil to the free surface strengthens this effect, resulting in more pronounced cavitation and increased fluctuations in the hysteresis performance.

Funding This work was supported by National Natural Science Foundation of China Grants (No. 91852117). It was also funded by the China Scholarship Council (No. 202108310159).

Declarations

Conflict of interest The authors declare that they have no conflict of interest.

References

1. Wu X, Zhang X, Tian X et al (2020) A review on fluid dynamics of flapping foils. Ocean Eng 195:106712
2. Mo W, He G, Wang J et al (2022) Hydrodynamic analysis of three oscillating hydrofoils with wing-in-ground effect on power extraction performance. Ocean Eng 246:110642
3. Zhu B, Cheng W, Geng J et al (2022) Energy-harvesting characteristics of flapping wings with the free-surface effect. J Renew Sustain Energy 14(1):014501
4. Che B, Chu N, Schmidt SJ et al (2019) Control effect of micro vortex generators on leading edge of attached cavitation. Phys Fluids 31(4):044102
5. Sezen S, Uzun D, Turan O et al (2021) Influence of roughness on propeller performance with a view to mitigating tip vortex cavitation. Ocean Eng 239:109703
6. Shengwang ZHU, Guijian X, Yi HE et al (2022) Tip vortex cavitation of propeller bionic noise reduction surface based on precision abrasive belt grinding. J Adv Manuf Sci Technol 2(1):2022003–2022003
7. Amromin E (2014) Development and validation of computational fluid dynamics models for initial stages of cavitation. J Fluids Eng. https://doi.org/10.1115/1.4026883
8. Sun T, Wei Y, Zou L et al (2019) Numerical investigation on the unsteady cavitation shedding dynamics over a hydrofoil in thermo-sensitive fluid. Int J Multiph Flow 111:82–100
9. Ji B, Luo XW, Arndt REA et al (2015) Large eddy simulation and theoretical investigations of the transient cavitating vortical flow structure around a NACA66 hydrofoil. Int J Multiph Flow 68:121–134
10. Zhao X, Cheng H, Ji B (2022) LES investigation of the cavitating hydrofoils with various wavy leading edges. Ocean Eng 243:110331
11. Timoshevskiy MV, Zapryagaev II, Pervunin KS et al (2018) Manipulating cavitation by a wall jet: experiments on a 2D hydrofoil. Int J Multiph Flow 99:312–328
12. Wang W, Tang T, Zhang QD et al (2020) Effect of water injection on the cavitation control: experiments on a NACA66 (MOD) hydrofoil. Acta Mech Sin 36(5):999–1017
13. Hart DP, Brennen CE, Acosta AJ (1990) Observations of cavitation on a three-dimensional oscillating hydrofoil
14. Ducoin A, Astolfi JA, Deniset F et al (2009) Computational and experimental investigation of flow over a transient pitching hydrofoil. Eur J Mech B/Fluids 28(6):728–743
15. Amromin E, Kovinskaya S (2000) Vibration of cavitating elastic wing in a periodically perturbed flow: excitation of subharmonics. J Fluids Struct 14(5):735–751
16. Huang B, Ducoin A, Young YL (2013) Physical and numerical investigation of cavitating flows around a pitching hydrofoil. Phys Fluids 25(10):102109
17. Kashyap SR, Jaiman RK (2023) Unsteady cavitation dynamics and frequency lock-in of a freely vibrating hydrofoil at high Reynolds number. Int J Multiph Flow 158:104276
18. Wu PC, Chen JH (2016) Numerical study on cavitating flow due to a hydrofoil near a free surface. J Ocean Eng Sci 1(3):238–245
19. Zhang M, Wu Q, Huang B et al (2018) Lagrangian-based numerical investigation of aerodynamic performance of an oscillating foil. Acta Mech Sin 34(5):839–854
20. Wu Q, Huang B, Wang G (2016) Lagrangian-based investigation of the transient flow structures around a pitching hydrofoil. Acta Mech Sin 32(1):64–74
21. Wu Q, Wang G, Huang B (2014) Numerical study of flow around oscillating hydrofoil and its transition characteristics. Chin J Theor Appl Mech 46(1):60–69
22. Zhang M, Feng F, Wang M et al (2022) Investigation of hysteresis effect of cavitating flow over a pitching Clark-Y hydrofoil. Acta Mech Sin 38(6):321382
23. Zhu B, Tai Z, Du D et al (2022) Effect of incoming gravity waves on the energy extraction efficiency of flapping wing hydroelectric generators. Ocean Eng 245:110590
24. Liu C, He J (2018) Improved application of Coupled algorithm in airfoil aerodynamic performance calculation. Sci Technol Eng 18(2):174–179
25. Zhang R, Zhao J, Guo S (2016) Numerical simulation of airfoil dynamic aerodynamics and analysis of its influencing factors. Aeronaut Comput Tech 46(04):75–77+82
26. Jiao Y, Fan J, Luo S (2011) Research on calculation of flow unsteadiness of multi-element airfoils. Sci Technol Eng 11(13):2994–2998
27. McCroskey WJ, McAlister KW, Carr LW et al (1982) An experimental study of dynamic stall on advanced airfoil sections. Volume 1. Summary of the experiment. National Aeronuatics and Space Administration Moffett Field Ca Ames Research Center
28. Guilmineau E, Piquet J, Queutey P (1997) Unsteady two-dimensional turbulent viscous flow past aerofoils. Int J Numer Methods Fluids 25(3):315–366
29. Duncan JH (1983) The breaking and non-breaking wave resistance of a two-dimensional hydrofoil. J Fluid Mech 126:507–520